ACS APPLIED MATERIALS & INTERFACES

Research Article

www.acsami.org

Structural, Chemical, Optical, and Electrical Evolution of SnO_x Films Deposited by Reactive rf Magnetron Sputtering

Hao Luo, Ling Yan Liang,* Hong Tao Cao,* Zhi Min Liu, and Fei Zhuge

Division of Functional Materials and Nano Devices, Ningbo Institute of Material Technology and Engineering, Chinese Academy of Sciences, Ningbo 315201, People's Republic of China

ABSTRACT: In this paper, SnO_x films were produced by reactive radio frequency magnetron sputtering under various oxygen partial pressure (P_O) in conjunction with a thermal annealing at 200 °C afterwards. The obtained SnO_x films were systematically studied by means of various techniques, including X-ray diffraction, Raman spectroscopy, X-ray photoelectron spectroscopy, spectroscopic ellipsometry, and Hall-effect measurement. The structural, chemical, and electrical evolution of the SnO_x films was found to experience three stages: polycrystalline SnO phase dominated section with p-type conduction at $P_O \leq 9.9\%$; amorphous SnO_2 phase dominated area at $P_O \geq 12.3\%$, exhibiting n-type characteristics; and conductivity dilemma area in between the above mentioned sections, featuring the coexistence of SnO and SnO_2 phases with compatible and opposite contribution to the conductivity. The polycrystalline to amorphous film structure transition was ascribed to the enhanced crystallization temperature due to the perturbed structural disorder by incorporating Sn^{4+} into the SnO matrix. The inversion from p-type to n-type conduction with P_O variation is believed to result from the competition between the donor and acceptor generation process, i.e., the n-type behavior would be present if the donor effect is overwhelming, and vice versa. In addition, with increasing P_O, the refractive index decreased from 3.0 to 1.8 and the band gaps increased from 1.5 to 3.5 eV, respectively.

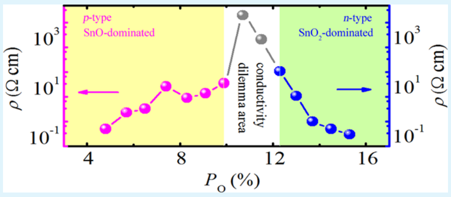

KEYWORDS: *SnO_2, SnO, reactive magnetron sputtering, XRD, XPS, Raman, ellipsometry, Hall effect*

INTRODUCTION

Stannic oxide (SnO_2), because of its excellent n-type semiconductor with low electrical resistance and high optical transparency in the visible range, is widely explored in various applications, such as transparent electrodes,[1] n-type thin film transistors (TFTs),[2] solar cells,[3] gas sensors,[4] etc. As another important tin oxide, stannous oxide (SnO) has also attracted ever-increasing attention for the applications as active layer in gas sensors,[5,6] as anode material for lithium rechargeable batteries,[7−9] and as a precursor for the production of SnO_2.[10] Especially, p-type TFTs have been fabricated by using SnO as p-channel material,[11−14] and ambipolar SnO TFTs have been demonstrated by controlling the channel thickness.[15] Very recently, we reported SnO-based ambipolar TFTs as well as ambipolar inverters, manifesting that the stoichiometry of the nominal SnO has a big impact on the ambipolar symmetry of the TFTs.[16]

Tin oxides (SnO_x) films can be prepared by various techniques, such as electron beam evaporation,[12] pulsed laser deposition,[13] chemical vapor deposition,[17] aqueous solution process,[18] hydrothermal synthesis,[19] magnetron sputtering,[11,20,21] etc., among which magnetron sputtering technique was utilized intensively. But whereas, most of research endeavors on tin oxides were mainly focused not on SnO, but on SnO_2 or foreign element doped SnO_2. Muranaka et al.[20] and Beensh et al.[21] respectively produced SnO_x films by magnetron sputtering using Sn metallic target at different oxygen partial pressure, and in particular, β-Sn and α-SnO phases were obtained at low oxygen partial pressure. However, their main concerns were on the performance of SnO_2 films, without systematically studying on the physical properties of SnO. Recently, Fortunato et al.[11] prepared p-type SnO_x films by reactive rf magnetron sputtering at different oxygen partial pressure for the usage of TFT channels, but a thorough investigation of the material's properties is still lacking.

In this study, SnO_x films were fabricated by reactive rf magnetron sputtering through controlling the oxygen partial pressure, and the structural, chemical, optical, and electrical properties of the films were comprehensively investigated. The results can provide a robust addition to the knowledge base for the fabrication and the physical properties of SnO_x films, which is indispensable whether for the fundamental research or the market-driven applications.

EXPERIMENTAL SECTION

A series of SnO_x films were prepared on quartz glasses by reactive rf magnetron sputtering, applying a 2 in. Sn metallic target (99.99%) at a power of 60 W. Prior to deposition, the substrates were cleaned by organic solvents (alcohol and acetone), deionized H_2O, and subsequently dried in N_2 gas flow. After evacuating below 1×10^{-4} Pa, SnO_x films were deposited at room temperature through controlling the O_2 and Ar gas flux at a constant working pressure of 0.46 Pa. The oxygen partial pressure P_O ($P_O = O_2/(O_2+Ar)\%$) varied from 4.8 to 15.3%. Films with a thickness in the range of 190−230 nm were obtained by fixing the deposition time for 30 minutes. The film

Received: August 9, 2012
Accepted: October 1, 2012
Published: October 1, 2012

thickness increases monotonously with P_O due to more O_2-induced weight and volume variation.[20] Finally, the as-deposited SnO_x films were subjected to a thermal annealing at 200 °C for 2 h in air.

The phase composition of the films was characterized by X-ray diffraction (XRD, Bruker D8 Advance X-ray diffractometer) with Cu K_α radiation. The microstructure was elucidated by a confocal microscope Raman spectrometer (Renishaw inVia-Reflex) using a 532 nm excitation line which is created by second harmonic generation (SHG) element from a line of 1064 nm generated by Nd:YAG laser. The wavenumber is changed from 50 to 900 cm^{-1} and the light-spot size is about 1 μm in diameter. The chemical composition was examined by X-ray photoelectron spectroscopy (XPS, Kratos Analytical Ltd., UK) using Al−K_α radiation. The optical properties were analyzed on a spectroscopic ellipsometry (SE, J.A. Woollam Inc.) in the range of 300−1700 nm. The electrical measurements were carried out at room temperature using a Hall-effect measurement system (HL5500).

RESULTS AND DISCUSSION

Phase and Microstructure Characteristics. Figure 1 shows the XRD patterns of the SnO_x films at various P_O. At P_O = 4.8%, both α-SnO phase (α-PbO structure, P4/nmm, JCPDS card No.06-0395) and β-Sn phase ($I4_1$/amd, JCPDS card No.19-1365) were observed in the films, but the former one dominated. As P_O increased, the intensity of β-Sn phase tapered and disappeared eventually at P_O = 6.5%, in completely contrast to the variation trend of α-SnO phase. As P_O changed from 6.5 to 9.9%, only α-SnO phase with more attenuated peak intensity was observed. When $P_O \geq$ 10.7%, there were no characteristic peaks for any phases perceived, suggesting the amorphous nature the films.

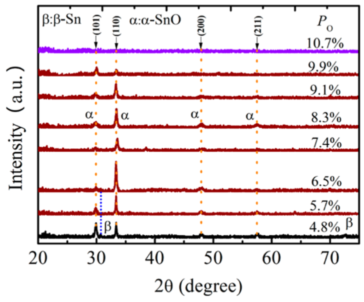

Figure 1. XRD patterns of the SnO_x films deposited at different oxygen partial pressure (P_O).

Raman measurements were utilized to identify Raman active phonon modes of the films, as displayed in Figure 2. Only two peaks located at 112 and 210 cm^{-1} which were indexed to the vibrational modes of SnO were observed for the polycrystalline SnO_x films ($P_O \leq$ 9.9%), whereas no Raman-active mode (~42.4 and 126.6 cm^{-1})[22−24] of β-Sn was present for the films even with the highest metallic Sn content (P_O = 4.8%), which is probably related to the intensive light absorption caused by the metallic particles or/and clusters. Moreover, no SnO_2 characteristic peaks (~474, 632, 774 cm^{-1})[25,26] were identified as well. SnO_2 phase, if presented and dominated at higher P_O (≥10.7%), is still in the amorphous format, because 200 °C is too low to make SnO_2 crystallized (>400 °C).[27] As shown in Figure 2, the Raman characteristic peaks disappeared completely at $P_O \geq$ 10.7% as the polycrystalline films were converted into amorphous ones. As a result, it is reasonably believed that the phonon scattering volume related to SnO_2 in this case is under the observation threshold of the Raman equipment. The designation of the two observed characteristic peaks of SnO will be discussed in the following.

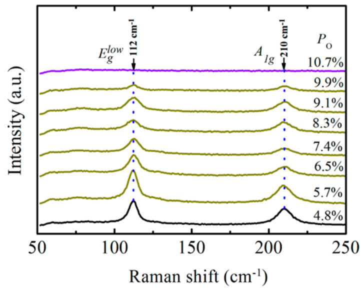

Figure 2. Raman spectra of the SnO_x films fabricated at various oxygen partial pressure (P_O).

The vibrational modes of SnO described by the group theory can be expressed as follows:[28]

$$\Gamma = A_{1g} + B_{1g} + 2E_g + A_{2u} + E_u + 3 \text{ acoustic modes} \tag{1}$$

of which A_{1g}, B_{1g}, E_g are Raman active, whereas A_{2u}, E_u are infrared-related modes. Figure 3 manifests the atomic displacements of A_{1g}, B_{1g}, and E_g modes. A_{1g} mode is polarized in the z direction, in which Sn atoms are vibrating along z axis toward or away from the x−y plane. B_{1g} mode is also polarized in the z direction, but the O atoms are vibrating out of the x−y plane. By comparison, two E_g modes, which are polarized within the x−y plane, involve vibrations within each sublattice and of one sublattice with respect to the other, respectively.[24] The peak at 210 cm^{-1} was assigned to A_{1g} mode definitely, in line with the theoretical calculations and experimental reports.[24,28,29] However, there is a bifurcation on the identification of the peak at 112 cm^{-1}. Geurts et al. believed that this peak can be ascribed to the B_{1g} mode.[28] The phonon frequency of B_{1g} was calculated to be 370, 350, and 357 cm^{-1} through ab initio full-potential linear-muffin-tin-orbital method, linear augmented-plane-wave calculation, and shell model, respectively.[24,29] Moreover, it is unreasonable that B_{1g} has a frequency (ω) lower than A_{1g}, considering that the mass (m) of O is smaller than Sn, because B_{1g} and A_{1g} modes are, respectively, O and Sn displacements, as the schematic illustrated in Figure 3 (in this case, $\omega \approx m^{-1/2}$).[24] In fact, the phonon frequency of E_g^{low} ranges from 113 to 143 cm^{-1} on the basis of the theoretical calculations. Thus, it is logically believed that the Raman peak at 112 cm^{-1} should be allotted to the low frequency E_g^{low} mode.

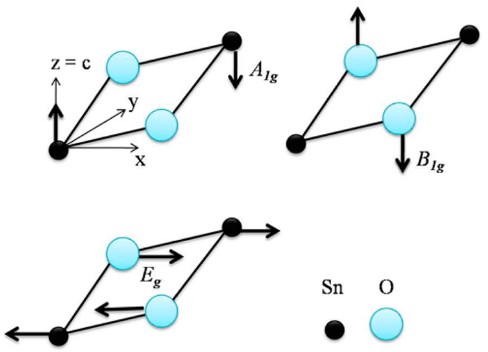

Figure 3. Schematic diagram to describe the atomic displacements of A_{1g}, B_{1g}, and E_g vibrating modes.

Chemical Composition Analysis. XPS measurements were performed to further confirm the chemical composition of the films. High doses of argon ions (Ion energy of 2 KeV, current density of 5 μA/cm^2 roughly) were used to sputter away the outmost layer, to get rid of the carbon contamination as well as the hydrated layer so as to obtain the actual composition of the SnO_x films. The binding energy data were calibrated with respect to the C1s signal of ambient hydrocarbons (C−H and C−C) at 284.8 eV.

Panels a and b in Figure 4 illustrate the typical core-level spectra of Sn 3d and O 1s, respectively. At P_O = 4.8%, the Sn 3d spectrum depicts a spin-orbit doublet peak located at ∼485.9 eV (Sn^{2+} $3d_{5/2}$) and ∼494.3 eV (Sn^{2+} $3d_{3/2}$) with two shoulders centered at ∼484.4 eV (Sn^0 $3d_{5/2}$) and ∼492.8 eV (Sn^0 $3d_{3/2}$). As P_O increased, the two shoulders gradually disappeared, whereas the chief peaks shifted to higher binding energies due to the presence of Sn^{4+} (486.6 eV and 495.0 eV for $3d_{5/2}$ and $3d_{3/2}$, respectively). Along with continuously increasing P_O, the content of Sn^{4+} became more and more, and gradually dominated at $P_O \geq$ 12.3%. Correspondingly, the evolution of O 1s spectra agrees well with that of Sn 3d spectra, as shown in Figure 4b. At P_O = 4.8%, the O 1s spectrum only showed one peak at 529.8 eV assigned to O−Sn^{2+}. As P_O increased, another peak centered at 530.4 eV (O−Sn^{4+}) presented and gradually became dominant. The binding energies of all the components in this experiment are consistent with the previously reported values.[30,31]

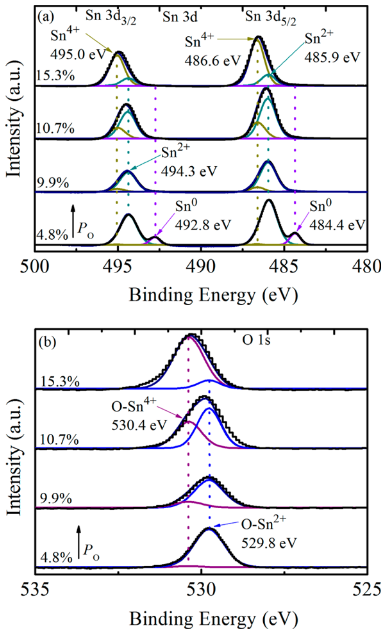

Figure 4. XPS spectra of (a) Sn 3d and (b) O 1s for the SnO_x films under various oxygen partial pressure (P_O). Step lines and smooth lines are representing raw data and fitting data, respectively.

The contents of SnO_2, SnO, and Sn in the SnO_x films were respectively calculated and illustrated in Figure 5. As P_O increased to 6.5%, the Sn content decreased from ∼14% to 0 nearly, whereas the SnO content increased to a maximum value (∼96%), in a good agreement with the XRD observation that the β-Sn phase faded away and the α-SnO-related peaks stretched out significantly. After that, the SnO content dropped persistently, approaching ∼18% at P_O = 15.3%, whereas the SnO_2 content increased from 0 till ∼82% with P_O. Moreover, it was noted that, a crystallization transition from polycrystalline to amorphous was confirmed by XRD technique at P_O = 10.7%, at which the SnO_2 content was ∼27%. In other words, although having considerably high crystallization temperature (> 400°C).[27] SnO_2 was not the dominant phase at P_O = 10.7% so that itself could not account for the crystallization transition exclusively. It is suggested that the involvement of Sn^{4+} boosted the structural disorder in the SnO_x matrix since Sn^{4+}−O and Sn^{2+}−O bonds have distinct coordination number, bond angle, and bond length, and so on, consequently improving the crystallization temperature.

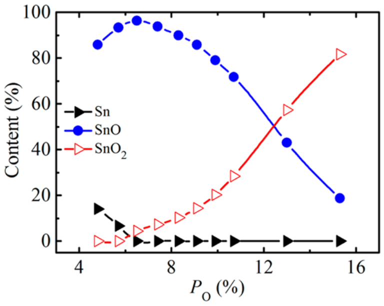

Figure 5. Content evolution of SnO_2, SnO, and Sn in the films as a function of oxygen partial pressure (P_O).

Optical Properties. Optical constants were obtained by fitting the SE data in the wavelength range of 300−1700 nm. Tauc-Lorentz dispersion function was employed to generate the refractive index n and extinction coefficient κ of the transparent films.[32] For films deposited at low P_O with low transmittance, effective medium approximate (EMA) layer model with the intervention of metal tin layer was used to generate the optical constants. The EMA approach, as a very robust approach to describe the electromagnetic response of the heterogeneous system when the feature size of the nonuniform composition is smaller than the wavelength, is based on the Lorentz cavity concept for the determination of the polarizability of an individual inclusion and Clausius-Mossotti relation.[33]

Figure 6a presents the refractive index of the films with P_O. For clarity, the refractive index at 550 nm was selected and plotted in the inset of Figure 6a. At P_O = 4.8%, the films with β-Sn and α-SnO phases involved showed a lower refractive index than α-SnO dominated films in the short wavelength range (<400 nm), simply owing to the smaller refractive index of β-Sn (0.37−1.0) in such range.[34] Whereas the refractive index of β-Sn increases dramatically with wavelength, for example, approaching ∼3.15 at 930 nm.[34] Thus the films incorporated with β-Sn phase presented higher refractive index in the long wavelength range (greater than ∼500 nm). With increasing P_O, however, the refractive index of the films decreased gradually, which was attributed to the increasing content evolution of SnO_2.[12] As reported, SnO_2 has a smaller refractive index (1.7−2.0 at 550 nm) than SnO (2.5−2.8 at 550 nm).[32,35,36] As expected in our experiment, the SnO-dominated films ($P_O \leq$ 9.9%) exhibited a refractive index (2.3−3.0 at 550 nm) higher than the SnO_2-dominated ($P_O \geq$ 12.3%) films (1.8−2.0 at 550 nm).

Optical band gaps E_{gap} of the films were obtained on the basis of a graphical method (as shown in Figure 6b) using the following equation

$$(\alpha h\nu)^2 = A(h\nu - E_{gap}) \qquad (2)$$

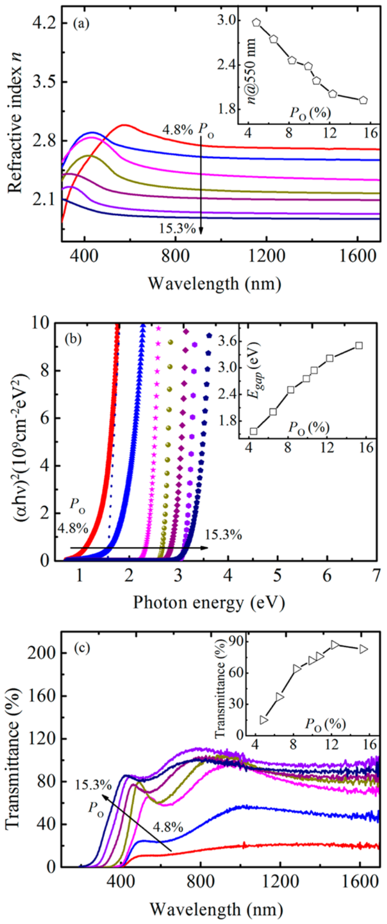

Figure 6. (a) Refractive index of the SnO_x films under different oxygen partial pressure (P_O) as a function of wavelength. Inset is the refractive index at wavelength 550 nm vs. oxygen partial pressure. (b) $(\alpha h\nu)^2$ as a function of photon energy $h\nu$. Inset is the calculated band gap vs. oxygen partial pressure. (c) The transmittance spectra of the SnO_x films with different oxygen partial pressure (P_O). Inset shows the average transmittance of the films.

where α is the absorption coefficient calculated via $\alpha = 4\pi\kappa/\lambda$ (λ is the wavelength of incident light), and A is a constant. The films at low P_O have a very narrow band gap (1.5−2.0 eV), because β-Sn phase, acting as metallic particles or clusters, absorbs the light intensively. As P_O increased, the E_{gap} values of the films increased almost linearly (as presented in the inset of Figure 6b) from 2.0 to 3.5 eV because there is more SnO_2 available, because SnO_2 (3.6 eV) has a broader band gap than SnO (2.5−2.8 eV).[28]

Figure 6c shows the transmittance spectra of the films measured by SE at different P_O. As expected, the films with β-Sn phase included displayed a low transmittance in the whole spectra because of the intensive light absorption of the metal ingredient. The films without β-Sn phase incorporated illustrated a marginal difference in the transmittance at long wavelength (>800 nm), whereas the band edge shifted gradually to the shorter wavelengths as P_O increased, which was consistent with the blue-shift of the band gaps. Hence, the average transmittance first increased rapidly and then tended to be saturated around 87% as P_O varied (as shown in the inset of Figure 6c).

Electrical Performances. Figure 7 manifests the dependence of resistivity, Hall mobility and carrier concentration on different P_O. The SnO-dominated films ($P_O \leq 9.9\%$) exhibited p-type conduction behavior with the mobility, the hole concentration, and the resistivity in the range of 0.3−1.3 $cm^2/(V\ s)$, 1×10^{17} to 1×10^{20} cm^{-3}, and 0.5−35 Ω cm, respectively. Generally speaking, the hole concentration displayed a decreasing trend with increasing P_O in the range of 4.8−9.9%. On the basis of first-principle calculations, the p-type conductivity of SnO films originates from the excess of oxygen or/and the tin vacancy (V_{Sn});[37] meanwhile, experimental results also confirmed that a SnO film with a high O/Sn ratio favors the formation of acceptors V_{Sn}, which thus produces more mobile holes.[38] However, this suggestion can not interpret the decreasing trend of the hole concentration in the SnO-dominated films, instead a carrier compensation effect is believed to account for that. According to the XPS results, a certain amount of Sn^{4+} ions were involved into the SnO-dominated films yet, and the Sn^{4+} content increased persistently with P_O. It is speculated that, the Sn^{4+} ion and/or its relate defect state acting as donors or hole killers, would compensate and/or capture a portion of free holes generated in the SnO-dominated films, consequently the hole concentration dropped with increasing P_O. When the number of free electrons has approximately the same order of magnitude with the free holes, the SnO_x films would display the maximum resistivity, which were observed for the films at P_O around 10.7% as named "conductivity dilemma area". The carrier concentration and mobility of the films fabricated at P_O = 10.7% and 11.5% were not available because of their high resistivity (~1×10^4 Ω cm), which is beyond the capability of the Hall-effect measurement. As P_O kept increasing, a conductivity inversion from p- to n-type was observed. For example, when P_O ranged from 12.3 to 15.3%, the SnO_2-dominated films demonstrated n-type conduction behavior unambiguously with a mobility in the range of 0.5−1.3 $cm^2/(V\ s)$, an increasing electron concentration ranging from 1×10^{17} to 1×10^{19} cm^{-3}, and a decreasing resistivity from 108 to 0.3 Ω cm, respectively.

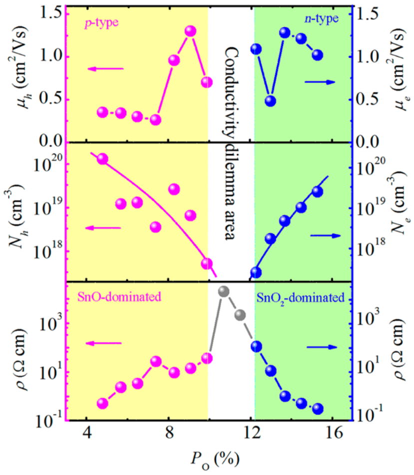

Figure 7. Resistivity ρ, hole/electron concentration N_h/N_e, and hole/electron mobility μ_h/μ_e vs. oxygen partial pressure (P_O).

CONCLUSION

SnO_x films were fabricated by reactive rf magnetron sputtering followed by a low temperature annealing at 200 °C, and the influence of oxygen partial pressure (P_O) on the various properties of the films was systematically investigated. It can be roughly divided into three P_O regions to describe the structural and electrical evolution of the films: (1) $P_O \leq 9.9\%$, the films presented a p-type conduction, in which polycrystalline SnO phase dominated. (2) $9.9\% < P_O < 12.3\%$, the films exhibited a characteristic of "conductivity dilemma area", where the crystallization temperature was improved so that a transition from polycrystalline to amorphous occurred, because the involvement of Sn^{4+} augmented the structural disorder in the SnO_x matrix. (3) $P_O \geq 12.3\%$, the films displayed an n-type behavior with increasing electron concentration as P_O increased, in which amorphous SnO_2 phase took the privileges. Moreover, the optical parameters presented a monotonic variation with increasing P_O, i.e., the refractive index decreased from 3.0 to 1.8 and the band gap increased from 1.5 to 3.5 eV, because of increasing content evolution of SnO_2. These results supply a comprehensive investigation on the structural, chemical, optical, and electrical property evolutions for the community of tin oxides, which would offer an opportunity to boost their further exploration and development.

■ AUTHOR INFORMATION

Corresponding Author

*E-mail: h_cao@nimte.ac.cn (H.T.C.); lly@nimte.ac.cn (L.Y.L.).

Notes

The authors declare no competing financial interest.

■ ACKNOWLEDGMENTS

This work is supported by the Chinese National Program on Key Basic Research Project (2012CB933003), the National Natural Science Foundation of China (Grants 11104289 and 61274095), the Science and Technology Innovative Research Team of Ningbo Municipality (2009B21005), the Key Program for Science and Technology Innovative Team of Zhejiang Province (2010R50020), and Applied Research Funds for Public Welfare Project of Zhejiang Provience (2011C21030).

■ REFERENCES

(1) He, Y. S.; Campbell, J. C.; Murphy, R. C.; Arendt, M. F.; Swinnea, J. S. *J. Mater. Res.* **1993**, *8*, 3131−3134.

(2) Presley, R. E.; Munsee, C. L.; Park, C. H.; Hong, D.; Wager, J. F.; Keszler, D. A. *J. Phys. D* **2004**, *37*, 2810−2813.

(3) Ferrere, S.; Zaban, A.; Gsegg, B. A. *J. Phys. Chem. B* **1997**, *101*, 4490−4493.

(4) Leite, E. R.; Weber, I. T.; Longo, E.; Varela, J. A. *Adv. Mater.* **2000**, *12*, 965−968.

(5) Calderer, J.; Molinas, P.; Sueiras, J.; Llobet, E.; Vilanova, X.; Correig, X.; Masana, F.; Rodriguez, A. *Microelectron. Reliab.* **2000**, *40*, 807−810.

(6) Watson, J. *Sens. Actuators.* **1984**, *5*, 29−42.

(7) Odani, A.; Nimberger, A.; Markovsky, B.; Sominski, E.; Levi, E.; Kumar, V. G.; Motiei, M.; Gedanken, A.; Dan, P.; Aurbach, D. *J. Power Sources* **2003**, *119*, 517−521.

(8) Aurbach, D.; Nimberger, A.; Markovsky, B.; Levi, E.; Sominski, E.; Gedanken, A. *Chem. Mater.* **2002**, *14*, 4155−4163.

(9) Uchiyama, H.; Hosono, E.; Honma, I.; Zhou, H. S.; Imai, H. *Electrochem. Commun.* **2008**, *10*, 52−55.

(10) Pan, X. Q.; Fu, L. *J. Appl. Phys.* **2002**, *89*, 6048−6055.

(11) Fortunato, E.; Barros, R.; Barquinha, P.; Figueiredo, V.; Park, S. H. K.; Hwang, C. S.; Martins, R. *Appl. Phys. Lett.* **2010**, *97* (052105), 1−3.

(12) Liang, L. Y.; Liu, Z. M.; Cao, H. T.; Yu, Z.; Shi, Y. Y.; Chen, A. H.; Zhang, H. Z.; Fang, Y. Q.; Xi Lian Sun, X. L. *J. Electrochem. Soc.* **2010**, *157*, H598−H602.

(13) Ogo, Y.; Hiramatsu, H.; Nomura, K.; Yanagi, H.; Kamiya, T.; Hirano, M.; Hosono, H. *Appl. Phys. Lett.* **2008**, *93* (032113), 1−3.

(14) Martins, R.; Nathan, A.; Barros, R.; Pereira, L.; Barquinha, P.; Correia, N.; Costa, R.; Ahnood, A.; Ferreira, I.; Fortunato, E. *Adv. Mater.* **2011**, *23*, 4491−4496.

(15) Nomura, K.; Kamiya, T.; Hosono, H. *Adv. Mater.* **2011**, *23*, 3431−3434.

(16) Liang, L. Y.; Cao, H. T.; Chen, X. B.; Liu, Z. M.; Zhuge, F.; Luo, H.; Li, J.; Lu, Y. C.; Lu, W. *Appl. Phys. Lett.* **2012**, *100* (263502), 1−5.

(17) Kumar, B.; Lee, D. H.; Kim, S. H.; Yang, B.; Maeng, S.; Kim, S. W. *J. Phys. Chem. C.* **2010**, *114*, 11050−11055.

(18) Sakaushi, K.; Oaki, K.; Uchiyama, H.; Hosono, E.; Zhou, H. S.; Imai, H. *Small* **2010**, *6*, 776−781.

(19) Zubair Iqbal, M.; Wang, F. P.; Rafi, U. D.; Javed, Q. U. A.; Yasir Rafique, M.; Li, Y.; Li, P. F. *Mater. Lett.* **2012**, *68*, 409−412.

(20) Muranaka, S.; Bando, Y.; Takada, T. *Thin Solid Films* **1981**, *86*, 11−19.

(21) Beensh Marchwicka, G.; Stepniewska, L. K.; Misiuk, A. *Thin Solid Films* **1984**, *113*, 215−224.

(22) Olijnyk, H. *Phys. Rev. B* **1992**, *46*, 6589−6591.

(23) Lewis, S. P.; Cohen, M. L. *Phys. Rev. B* **1993**, *48*, 3646−3653.

(24) Peltzer y Blanca, E. L.; Svane, A.; Christensen, N. E.; Rodriguez, C. O.; Cappannini, O. M.; Moreno, M. S. *Phys. Rev. B* **1993**, *48*, 15712−15718.

(25) Sun, S. H.; Meng, G. W.; Zhang, G. X.; Gao, T.; Geng, B. Y.; Zhang, L. D.; Zuo, J. *Chem. Phys. Lett.* **2003**, *376*, 103−107.

(26) Chen, Z. W.; Lai, J. K. L.; Shek, C. H. *Phys. Rev. B* **2004**, *70* (165314), 1−7.

(27) Zenkyu, R.; Tauima, D.; Yuhara, J. *J. Appl. Phys.* **2012**, *111* (064907), 1−6.

(28) Geurts, J.; Rau, S.; Richter, W.; Schmitte, F. J. *Thin Solid Films* **1984**, *12*, 217−225.

(29) Koval, K.; Burriel, R.; Stachiotti, M. G.; Castro, M.; Migoni, R. L.; Moreno, M. S.; Varela, A.; Rodriguez, C. O. *Phys. Rev. B* **1999**, *60*, 14496−14499.

(30) Szuber, J.; Czempik, G.; Larciprete, R.; Koziej, D.; Adamowicz, B. *Thin Solid Films* **2001**, *391*, 198−203.

(31) Her, Y. C.; Wu, J. Y.; Lin, Y. R.; Tsai, S. Y. *Appl. Phys. Lett.* **2006**, *89* (043115), 1−3.

(32) Liang, L. Y.; Liu, Z. M.; Cao, H. T.; Shi, Y. Y.; Sun, X. L.; Yu, Z.; Chen, A. H.; Zhang, H. Z.; Fang, Y. Q. *ACS Appl Mater. Interfaces* **2010**, *2*, 1565−1568.

(33) Aspnes, D. E. *Am. J. Phys.* **1982**, *50*, 704−709.

(34) Palik, E. D. *Handbook of Optical Constants*; Academic Press: San Diego, 1998; Vol. 3, pp 271−274.

(35) Paulson, P. D.; Hegedus, S. S. *J. Appl. Phys.* **2004**, *96*, 5469−5477.

(36) Kim, T. W.; Lee, D. U.; Choo, D. C.; Kim, J. H.; Kim, H. J.; Jeong, J. H.; Jung, M.; Bahang, J. H.; Park, H. L.; Yoon, Y. S.; Kim, J. Y. *J. Phys. Chem. Solids* **2002**, *63*, 881−885.

(37) Togo, A.; Oba, F.; Tanaka, I.; Tatsumi, K. *Phys. Rev. B* **2006**, *74* (195128), 1−8.

(38) Guo, W.; Fu, L.; Zhang, Y.; Zhang, K.; Liang, L. Y.; Liu, Z. M.; Cao, H. T.; Pan, X. Q. *Appl. Phys. Lett.* **2010**, *96* (042113), 1−3.

■ NOTE ADDED AFTER ASAP PUBLICATION

This paper was published on the Web on October 11, with errors in the Synopsis and Abstract graphic. The corrected version was reposted on October 15, 2012.